A Coupled Solid-Fluid Method for Modeling Subduction

Klaus Regenauer-Lieb, Gabriele Morra

A Coupled Solid-Fluid Method for Modeling Subduction

Journal:	*Philosophical Magazine & Philosophical Magazine Letters*
Manuscript ID:	TPHM-05-Jun-0278
Journal Selection:	Philosophical Magazine
Date Submitted by the Author:	06-Jun-2005
Complete List of Authors:	Regenauer-Lieb, Klaus; Johannes Gutenberg University, Geosciences; CSIRO, Exploration and Mining Morra, Gabriele; ETH, Geophysics
Keywords:	multiscale simulation, computer modelling, FEM, mechanical behaviour, plasticity, rheology, geological materials, fluids
Keywords (user supplied):	

A Coupled Solid-Fluid Method for Modeling Subduction

Gabriele Morra[1]
Klaus Regenauer-Lieb[2,3]
[1] ETH Zurich, Institute of Geophysics, 8093 Zurich, Switzerland
[2] CSIRO Mining and Exploration, Perth, PO Box 1130, Bentley WA 6102
[3] Johannes Gutenberg University, Geophysics and Geodynamics, 55099 Mainz, Germany

May 27, 2005

Abstract

We present a novel dynamic approach for solid/fluid coupling by joining two different numerical methods: Boundary Element Method (BEM) and Finite Element Method (FEM). FEM results describe the thermo-mechanical evolution of the solid while the fluid is solved with the BEM. The bidirectional feedback between the two domains evolves along a Lagrangian interface where the FEM domain is embedded inside the BEM domain. The feedback between the two codes is based on the calculation of a specific drag tensor for each boundary/finite element. The approach is presented here to solve the complex problem of the descent of a cold subducting oceanic plate into a hot fluid like mantle. The coupling technique is shown to maintain the proper energy dissipation caused by the important secondary induced mantle flow induced by the lateral migrating of the subducting plate. We show how the method can be successfully applied for modelling the feedback between deformation of the oceanic plate and the induced mantle flow. We find that the mantle flow drag is singular at the edge of the retreating plate causing a distinct hook shape. In Nature such hooks can be observed at the northern end of the Tonga trench and at the southern South-American trench perimeter.

1 Introduction

Plate tectonics is a multi-scale process. On the scale of 660 km depth, plates are moving relatively fast owing to the low viscosity of the upper mantle. Within this

rapid near-adiabatic process, lateral temperature contrast is retained for at least half of the convection cycle. The feedback between cold and stiff slabs and the hot upper mantle is significant. Our aim is to formulate a fast numerical method capable of solving the full feed-back in 3-D between the plates and the induced upper mantle motion.

The full solution of the 3-D multi-scale mechanical equations from the dislocation to the Earth scale is presently impossible. The central problem thus shifts toward developing a mathematical formulation of the problem that can capture the basic, yet simplified physics. Several numerical and experimental approaches have been put forward to date.

i) Beginning with the largest planetary scale, the fluid-dynamic approximation is successful in reproducing emergence of plate tectonics out of basic convection [Davies, 1995, Bercovici, 1993, Moresi and Solomatov, 1998, Tao and O'Connell, 1993, Davies, 1995]. The assumption of a temperature dependent yield stress represented a breakthrough. It brought global convection approaches to match Earth-like plate distribution [Trompert and Hansen, 1998, Tackley, 2000a, Tackley, 2000b]. However when zooming into the individual subduction zones, this approach reveals limitations because it produces near vertical symmetric downwelling instead of asymmetric subduction features.

ii) Stepping down to subduction scale, different modeling approaches have been proposed: a) A fluid-dynamic approach where a predefined asymmetric structure is necessary to guide the subducting plate. This structure is either a weak fault e.g. [Zhong and Gurnis, 1995] or a surfacing asthenosphere [Christensen, 1996, Houseman and Gubbins, 1997, Schmeling et al., 1999, Cizkova et al., 2002]. b) Another type of models ignores the convecting mantle entirely treating the slab quasi-statically as a fully isolated solid-mechanical feature only supported by buoyancy forces [Yoshioka and Wortel, 1995, Hassani et al., 1997, Buiter et al., 1998].

The same separation into solid or fluid mechanical approaches also applies to laboratory models where a solid mechanical slab is supported by water, neglecting any viscous mantle drag [Shemenda, 1993] or two different viscous materials representing the lithosphere and the mantle are chosen e.g. [Kincaid and Olson, 1987, Kincaid and W., 2003]. Finally, hybrid laboratory experiments have been proposed joining the two approaches [Jacoby, 1973, Faccenna et al., 1999].

We present here the first such hybrid numerical method in geodynamics by coupling FEM and BEM solutions. The Lagrangian FEM results describe a moving boundary. Thus, the BEM which has a mesh only at the boundaries, is the most natural fluid-dynamic approach for the coupling. We present an original coupling technique inspired by low Reynolds number fluid-dynamics theory. [Happel and Brenner, 1983] have shown that the drag due to creeping flow can be described in tensorial form on the boundary. Our novel technique is based on the calculation of a specific

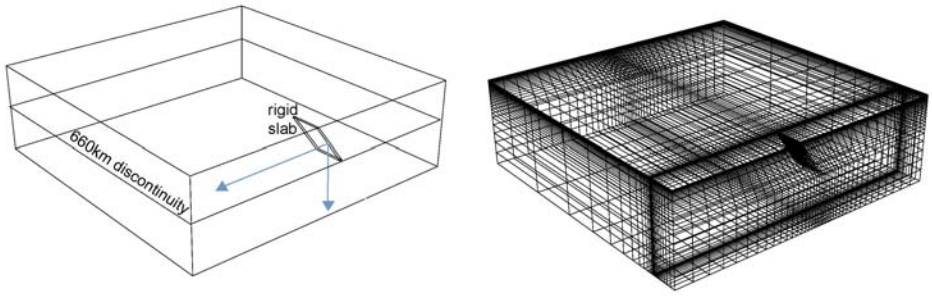

Figure 1: Set-up for the FEM model of instantaneous mantle flow. On the left the slab is immersed in the mantle. Arrows indicate the possible velocities of migration. On the right the FEM mesh, finer at the slab edges.

feedback tensor for each element. This approach allows a full dynamical coupling maintaining a good efficiency.

2 3-D Finite Element Models of Instantaneous Mantle Flow

When a subducting plate is migrating backwards, it produces a mantle flow which could influence (feed-back) the dynamics of the plate itself, changing the subduction-retreating velocity and/or its shape. In the next sections we present a coupled 3DFEM-2DBEM numerical implementation which offer important insights in the shape change due to this feed-back. In order to justify the assumption of 2-D (horizontal) toroidal mantle flow we calculate in this section instantaneous solutions for 3-D back-flow and show that for an horizontally migrating trench the back-flow is almost exclusively horizontal.

We use a FEM approach to calculate the effect of the presence of horizontal boundaries (surface and 660km discontinuity, the first assumed as impermeable free slip boundary, the second as sharp viscosity transition), on the mantle flow in a setup based on a rigid plate which moves horizontally and vertically in a laterally unbounded domain.

The drag on the plate can be estimated by the global mantle motion. Stokes flow theory shows that the total drag on immersed bodies is independent of the shape but simply proportional to the average size of the body (e.g. corner and cusp effects are negligible compared to the total drag, even if in proximity of the edge, the stress is singular). It is therefore possible to use a coarse FEM mesh to estimate

the large scale motion of the flow around the plate.

We first start with a set-up shown in figure 1. Symmetric boundary conditions at the centre of the plate and a better refined mesh in proximity to the edge of the slab are also implemented. We assume no-slip boundary conditions at the far-sides. At the surface free slip boundary condition is imposed, while a high viscosity contrast (factor of 30), as already proposed in previous work (e.g. [Funiciello et al., 2003a]), is assumed for the material below 660 km depth. The rheology is here only Newtonian, as the rheology implement within the Boundary Element Method presented in the next section. The flow is driven by kinematic pre-imposed plate velocity, once horizontally and once vertically. The plate cannot therefore change shape. The feed-back on the lithosphere dynamics will be analyzed in the following sections through the BEM-FEM approach. The solver is the same Lagrangian FEM solver described in the next section.

In figure 2, the horizontally migrating plate causes a back-flow, sideways to the plate, along parallel planes. This effect is mainly due to the horizontal boundaries (impermeable top surface and high viscosity transition at the 660km discontinuity). The drag on the plate therefore varies horizontally more then vertically. When the plate migrates horizontally the plate develops an arc shape controlled by the forcing of the back-flow and the resistance to bending of the plate. We will show in a later section how we use this result to apply the BEM/FEM method to the problem of gravity driven subduction.

Slab horizontal migration furthermore generates an eddy in proximity of the edge of the plate. This can be reproduced with an analytical solution of a point force in a 2-D unbounded fluid (Green function of Stokes equation, also called Stokeslet). When a plate that has already touched the 660km discontinuity migrates horizontally, also the back-flow migrates horizontally too. We tested the robustness of this result with different plate width and migration velocities.

A complex eddy has been suggested to be responsible for the genesis of mount Etna [Gvirtzman and Nur, 1999]. Here, slab migration at the triple junction of three plates may have generated a complex “toroidal plume” that could be visible at the surface as a volcanic edifice. Our approach can be used, in principle,to quantify the likely vigour of a toroidal eddy, if it is such a feature. However, we would like to point out at the same time that such extreme local restrictions warrant a much more detailed nonlinear temperature dependent implementation of the mantle rheology. A treatment of such cases, where extreme viscous dissipation in the fluid domain changes the rheological properties of creeping flow itself is beyond the scope this paper.

While the horizontally migrating plate produces mainly toroidal flow, the sinking plate effects are dominated by poloidal motion. In front of the trench a high velocity peak is produced, with the the maximum of velocity corresponding to the

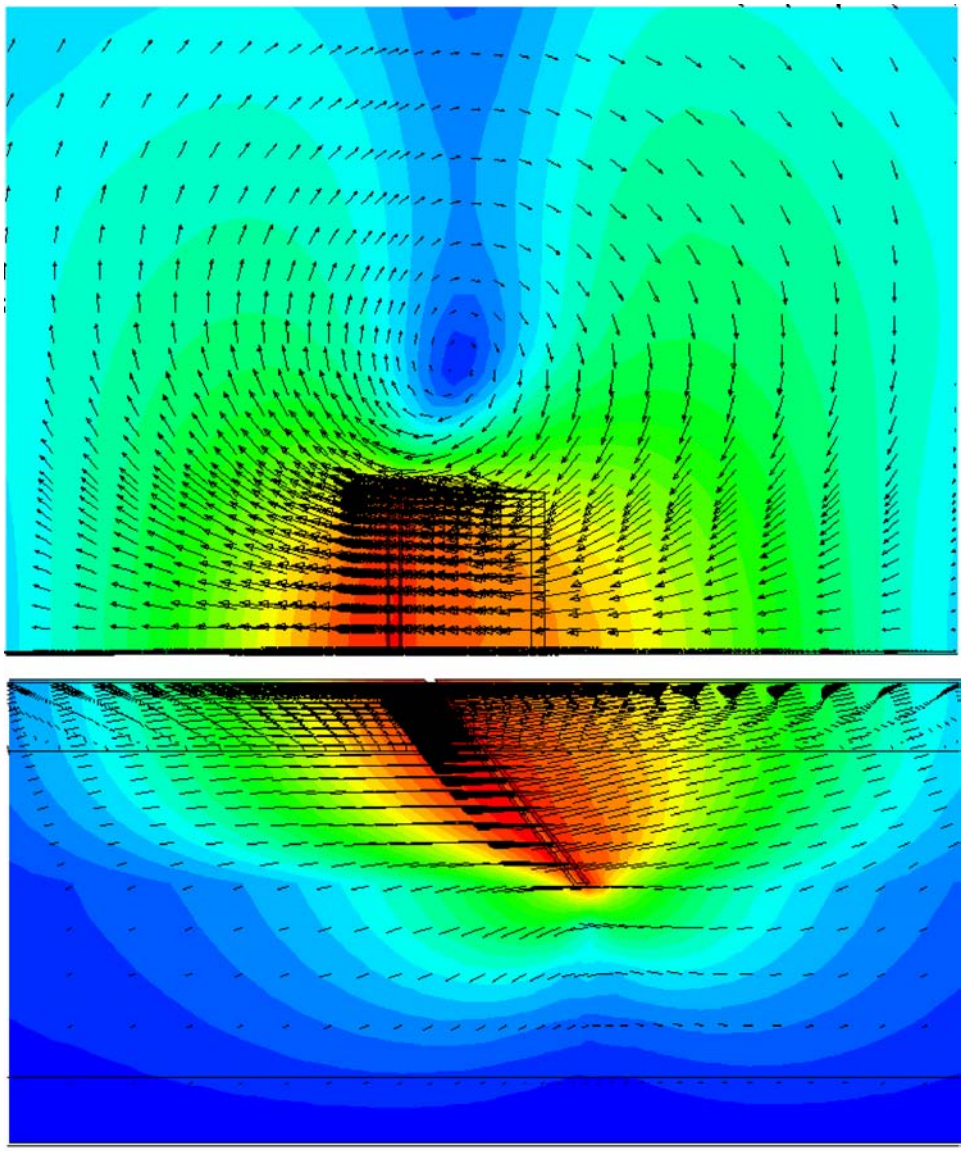

Figure 2: Mantle flow for a rigid plate migrating horizontally in a layered mantle (660km sharp viscosity discontinuity). Top: colors indicate velocity intensity and arrows show the direction. The length of the arrows is proportional to the intensity. Close to the lateral edge of the slab an eddy develops. This feature is common to all simulations with the same setup but different slab widths. Bottom: side view of the same quantities. We notice that the mantle back-flow is almost only horizontal

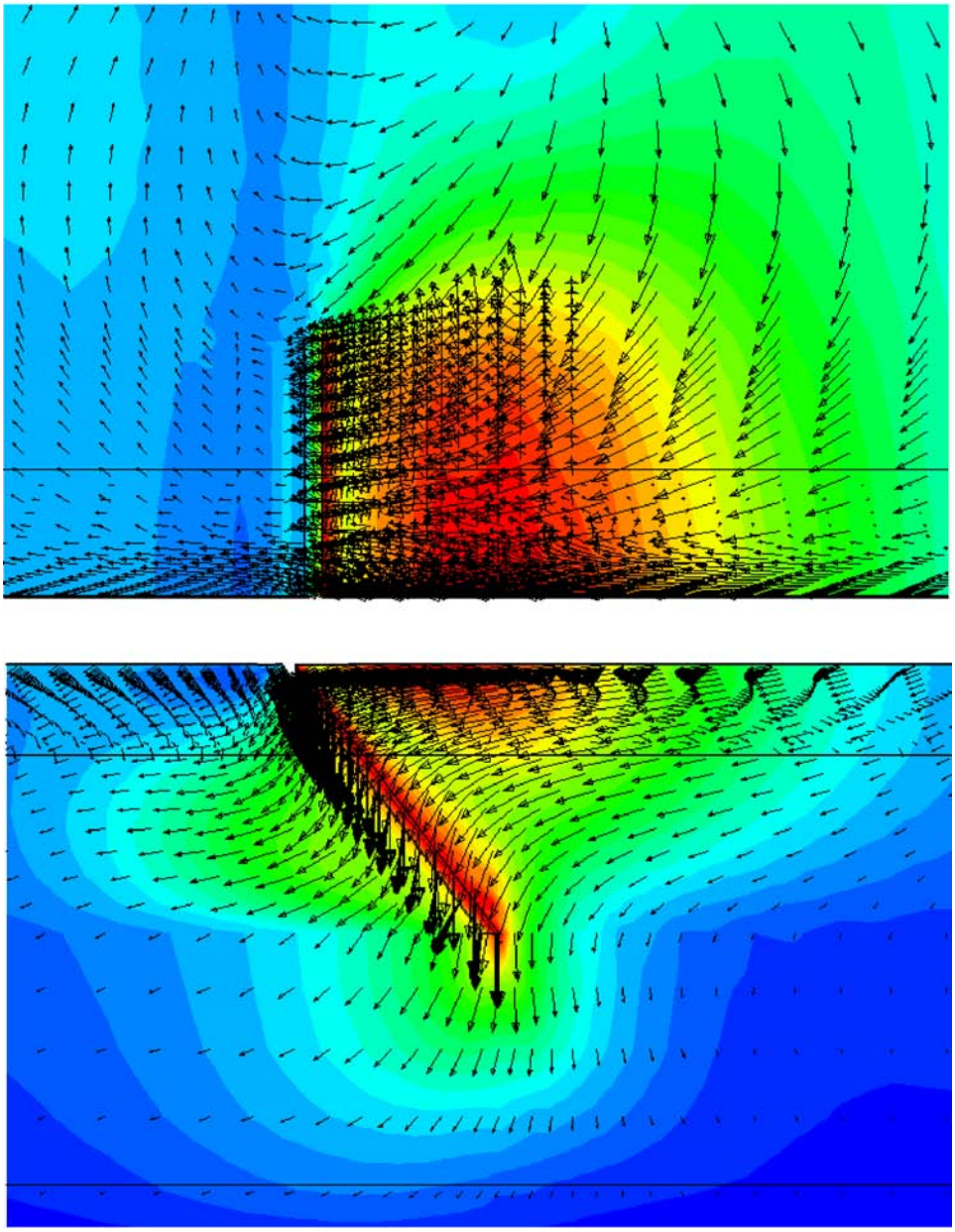

Figure 3: Mantle flow for a vertically migrating plate in a layered mantle (660km sharp viscosity discontinuity). Top: colors indicate velocity intensity and arrows show the direction. The length of the arrows is proportional to the intensity. Velocity intensity are much faster in front of the trench, where is the overriding plate (not modeled). Down: side view of the same quantities. Differently from fig. 2 the back flow is mostly poloidal.

point where the slab touches the 660 km discontinuity. This effect is naturally produced by the model and can be arguably correlated with the opening of a back-arc basin. However it is an open issue whether the opening is due to an up-flow from the mantle or due to suction of the corner flow.

3 Numerical methods

3.1 Finite Element Method (FEM) for Elasto-Plastic (Creep) Flow

The theory of finite element method is based on the virtual work principle. If $\delta\bar{u}$ are the admitted displacements (associated to $\delta\dot{\bar{\bar{\epsilon}}}$ admitted strain rate tensor variation), of a volume V embedded in the surface S with normal $\bar{n}$ to the surface, it reads:

$$\int_S \bar{n}\cdot\bar{\bar{\sigma}}\cdot\delta\bar{u}dS+\int_V \bar{f}\cdot\delta\bar{u}dV=\int_V \bar{\bar{\sigma}}:\delta\dot{\bar{\bar{\epsilon}}}dV \tag{1}$$

where $\bar{\bar{\sigma}}$ is the stress tensor and $\bar{f}$ a generic body force. If the solution in the domain V is approximated with N nodes each with k degrees of freedom, we can write:

$$\int_S \bar{n}\cdot\bar{\bar{\sigma}}\cdot\delta\bar{e}_i dS+\int_V \bar{f}\cdot\delta\bar{e}_i dV=\int_V\left(\frac{\partial\delta\bar{e}_i}{\partial\bar{x}}\right):\bar{\bar{\sigma}}dV\quad\forall i \tag{2}$$

where $\delta\bar{e}_i$ are now the admitted displacement projected along the i degree of freedom. Those Nk nonlinear equations form a system of equations that depends only on the virtual displacement u^i and can be thus written in the generic form $F^l\left(u^i\right)=0$, solvable employing an iterative algorithm.

We solve first the elastic equation, adopting a hypo-elastic assumption. Mantle and lithosphere rock creep can be in general expressed in a formulation written in function of an associate potential f as:

$$\frac{\Delta\bar{\bar{\epsilon}}^{cr}}{\Delta t}=\frac{\partial f}{\partial\bar{\bar{\sigma}}} \tag{3}$$

where $\bar{\bar{\epsilon}}^{cr}$ is the incremental creep strain in the time Δt. The resulting newton iterative equation is:

$$\delta(\bar{\bar{\epsilon}}^{cr})-\delta(\Delta t)\frac{\partial f}{\partial\bar{\bar{\sigma}}}-\Delta t\frac{\partial^2 f}{\partial\bar{\bar{\sigma}}\partial\bar{\bar{\sigma}}}:\delta(\Delta\sigma)=\Delta t\frac{\partial f}{\partial\bar{\bar{\sigma}}}-\Delta\bar{\bar{\epsilon}}^{cr} \tag{4}$$

this is is iterated until convergence is achieved.

3.2 Boundary Element Method (BEM) for Stokes Flow

Boundary element methodologies comprise a wide spectrum of techniques that, compared to FEM approaches, are much more complex from the mathematical point of view. This complexity is often compensated by a higher computational efficiency. For large domains BEM requires to mesh only the boundary of the domain, reducing drastically the size of the stiffness matrix. However the complexity of the analytical procedure required to build the BEM approach is sometimes not affordable. It is based on the analytical solution of the Green function of the equation to be computed and its integration (always singular) on the generic boundary element.

A short summary is given here, while a more extensive treatement of the BEM for Stokes Flow can be found in [Pozrikidis, 1992, Pozrikidis, 2002].

The Stokes equation is:

$$-\bar{\nabla}p + \mu\nabla^2\bar{u} + \rho\bar{b} = \bar{\nabla}\cdot\bar{\bar{\sigma}} + \rho\bar{b} = 0 \tag{5}$$

where $\bar{b}$ are the body forces. If we apply a singularity force to the system $\bar{f} = \bar{g}\delta\left(\bar{x} - \bar{x}_o\right)$, the solution will be the Green functions of the velocity, pressure and stress for the Stokes flow:

$$u_i(\bar{x}) = \frac{1}{8\pi\mu}G_{ij}(\bar{x},\bar{x}_o)g_j = \frac{1}{8\pi\mu}\left(\frac{\delta_{ij}}{r} + \frac{x_i x_j}{r^3}\right)g_j \tag{6}$$

$$p_i(\bar{x}) = \frac{1}{8\pi}P_j(\bar{x},\bar{x}_o)g_j = \frac{1}{4\pi}\frac{x_j}{r^3}g_j \tag{7}$$

$$e\sigma_{ik}(\bar{x}) = \frac{1}{8\pi}T_{ijk}(\bar{x},\bar{x}_o)g_j = \frac{3}{4\pi}\frac{x_i x_j x_k}{r^5}g_j \tag{8}$$

Invoking the Lorentz reciprocal identity $\frac{\partial}{\partial x_k}(u_i'\sigma_{ik} - u_i\sigma_{ik}') = 0$, it is possible to find a relationship between stress and velocity. Substituting the Green functions and expressing it in a infinitesimally small volume centered in x_o, one finds:

$$u_i(\bar{x}_o) = -\frac{1}{8\pi\mu}\int_D \bar{\bar{\sigma}}_{jk}(\bar{x})\bar{n}_k\bar{\bar{G}}_{ij}(\bar{x},\bar{x}_o)dS(\bar{x}) + \frac{1}{8\pi}\int_D \bar{u}_j(\bar{x})\bar{n}_k\bar{\bar{\bar{T}}}_{ijk}(\bar{x},\bar{x}_o)dS(\bar{x}) \tag{9}$$

where the first integral is known as "single layer" and the second as "double layer". The "single layer" physically represents the flow due to a surface distribution of point forces. The "double layer" represents the flow due to a surface distribution of particular stress tensor T, called stresslet. Those are the fundamental boundary equations for the Stokes Flow, expressed on the surface domain. The

solution for the BEM equation is also obtained through iteration on the discretized domain D, where normally only one of the two "layers" is solved, introducing effective quantities for $\bar{\bar{\sigma}}_{ik}$ or $\bar{u}_i$ on the integration points on D.

The limitation of boundary element method is that it requires the prior knowledge of the green functions, which is only available for simplified rheologies. This limitation is however compensated by computationally efficiency for large domains, because a significantly coarser incrementation than in FEM is necessary to mesh the domain boundary. Furthermore BEM is the best method for solving convex or concave geometry, corners, cusps or any other source of singular solution.

3.3 BEM and FEM 2-D Benchmark

BEM and the other integral approaches are the fastest and most precise approaches for solving elliptic homogeneous PDE's with constant coefficients. FEM on the other hand can be much easier applied to a wider variety of problems. We will now benchmark BEM and FEM in a simplified setting where analytical solutions are available.

Only few exact analytical solutions for Stokes flow are available in a bounded framework. We choose ones where the accuracy of BEM solutions to estimate singularities is put in evidence. The setup is shown in Figure 4. A circular infinitely long rod moves transversally inside a stationary circular cylinder. For this specific case Slezkin found an analytical solution for a rod that has a radius a much smaller than the cylinder radius b [Happel and Brenner, 1983]:

$$F = \frac{4\pi\mu U}{\ln\left(\frac{b}{a}\right) - 1} \tag{10}$$

where μ is the viscosity and U the velocity of motion of the rod. It is assumed that the shape of the rod remains rigidly circular during the motion and thus the energy is dissipated only in the fluid between the two cylinders. This analytical solution shows a typical characteristic of 2-D Stokes flow: the boundaries remain important even if they are far (e.g. b cannot be assumed infinite, otherwise $F = 0$).

BEM is the most suitable approach for calculating the effect of singular points. Figure 4 shows the benchmark results. Both our BEM and FEM codes reproduce the analytical solution for small radii. However the BEM method needs only 32 boundary elements while the FEM method necessitates 1500 elements and a finer mesh in proximity to the inner rod to get proper resolution for high ratios b/a. Within the FEM approach, furthermore, extra elements are necessary for higher ratios. On the contrary, BEM gives an equivalent precise result independently by b/a.

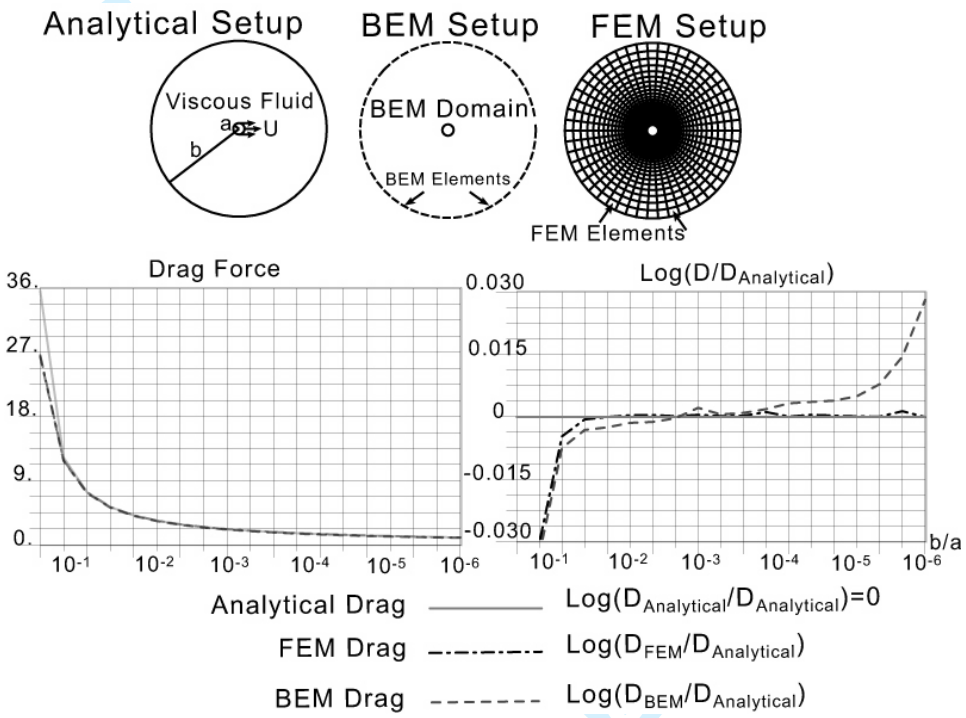

Figure 4: On the top the three different setups for analytical, BEM and FEM problems are represented. Each segment in the BEM setup represents one (circular) element. Each quadrilateral in the FEM setup represents one element. The bottom graphs show the drag force calculated with the three approaches. In the graph on the left panel the results for FEM and BEM are almost indistinguishable. On the right side the difference is plotted in logarithmic scale showing that BEM methods reproduce more exactly the case of a very thin rod. BEM seem thus more suitable for modeling edges and corners. Furthermore the BEM model required only N elements while FEM needs N^2.

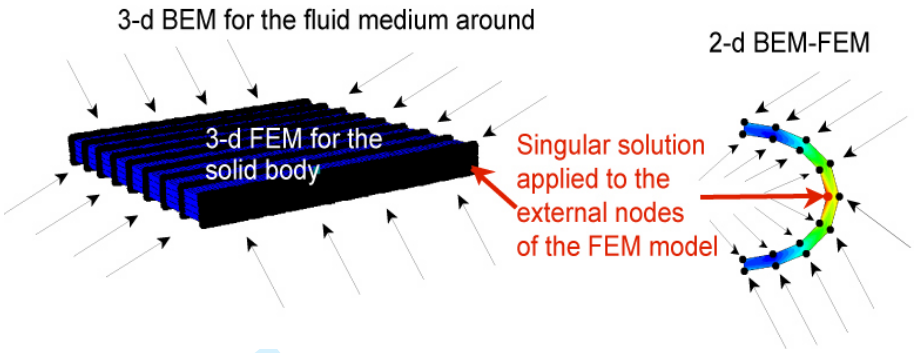

Figure 5: Sketch of 3-D and 2-D BEM FEM implementation. BEM solution is applied at the boundaries of the FEM domain as drag tensors, not as kinematic or dynamic boundary conditions.

4 The BEM - FEM Coupling

Assuming a body characterized by a complex rheology immersed in a Stokes fluid, we propose to couple the two applying the Finite Element Method to the Body and the Boundary Element Method to the surrounding fluid. A schematic plot of how BEM-FEM coupling in 2-D or 3-D can be implement is shown in figure 5. At the nodes located at the boundary between the two computational domains the BEM solution is applied as boundary condition of the FEM solution.

The evolving boundaries between the FEM and the BEM domains are characterized by a jump in stress (due to the different constitutive materials) but continuity in velocity. The difficulties in approximating properly the quantities at the boundary has caused many problems in different types of coupling approaches. The simplest and least computationally expensive method is the staggered one: to calculate velocities within the FEM framework, apply them to the BEM resulting in new drag forces. A second method, more sophisticate but also more exact, consists in matching all the physical quantities at the boundaries. Experience has shown that the first approach brings unstable processes that require very short time increments [Pozrikidis, 1992], while the second requires an iterative solution at the boundary that can be computationally very expensive and also sometimes requires short time increments.

For modeling the entire process of subduction we use a different coupling technique. The immersed material (lithosphere, modeled with FEM) is several orders of magnitude more viscous than the surrounding (mantle, modeled with BEM). A more sophisticated but also much more efficient approximation can be imple-

mented for the drag. During each increment the strain-rate (and therefore the variation of the momentum) of the lithosphere is much smaller then the mantle deformation. It is therefore possible to approximate its drag to the first order as that of a rigid body. The "pseudo-rigid" body shape will then slowly change in time. This approximation has the great advantage that the drag force can be written as product of a tensor (dyadic) and a velocity vector, for any shape of the semi-rigid body [Happel and Brenner, 1983].

We now show how to recover the equations for the FEM boundary, assuming the knowledge of the local drag tensors, obtained as a results of the BEM calculation. If the velocity $\bar{U} = \bar{u} + \bar{\omega} \times \bar{x}$, we can write force and torque fundamental solutions on a rigid body as:

$$\bar{F} = -\mu \bar{\bar{G}}_T \cdot \bar{u} \tag{11}$$

$$\bar{T} = -\mu \bar{\bar{G}}_R \cdot \bar{\omega} \tag{12}$$

where $\bar{F}$ is the force, $\bar{T}$ the torque, $\bar{\bar{G}}_T$ and $\bar{\bar{G}}_R$ respectively the translational and rotary force resistance tensors.

For a generic immersed deformable body, the above expressions can be rewritten within an integral framework [Pozrikidis, 1992], where the $\bar{\bar{G}}_T$ and $\bar{\bar{G}}_R$ tensors are now locally dependent by the position on the immersed body boundary:

$$\bar{F} = -\mu \int_S \bar{u} \cdot \bar{\bar{G}}_T(x) dS \tag{13}$$

$$\bar{T} = -\mu \int_S \bar{\omega} \cdot \bar{\bar{G}}_R(x) dS \tag{14}$$

For coupling BEM and FEM, the integral equations are simplified by the splitting of the integration surface in sub-domains, each representing an external face of a FEM element. The formulation of the resistance force applied at the boundary is thus:

$$\bar{F}\left(E_n\right) = -\mu \bar{\bar{G}}_{E_n} \cdot \int_{E_n} \bar{u}_{E_n} dS \tag{15}$$

where E_n is the external face of the n_{th} element, $\bar{\bar{G}}_{E_n}$ is calculated with the BEM approach and $\bar{u}_{E_n}$ is the solution found following for example an iterative scheme only within the FE Method.

The actual implementation is performed through "variable" point forces (dashpots) on the external nodes of the lithosphere. The value of the dashpots is dynamically calculated by the BEM solver, through the input of the shape of the FEM external mesh and its nodal velocities, respectively.

4.1 BEM-FEM Benchmark

The simple coupling approach presented above was benchmarked with several setups. We show one that has immediate application to subduction: a two-dimensional viscoelastic plate (modeled with FEM, $\eta = 10^{23} Pas$, $E = 10^{11} Pa$) that is subject to gravity and to a boundary drag by a weaker viscous medium (modeled with BEM, $\eta = 10^{21} Pas$). The effective viscosity contrast between the two domains is two orders of magnitude, therefore the approximation of semi-rigidity for the calculus of the drag is expected to work efficiently.

Before showing the results, we study the solution obtained by the BEM solver. The stress induced by a rigid straight plate that migrates in a fluid is singular at the plate edge, one has to be therefore cautious with its integration. Experience has shown that the accuracy of the computation degrades on a local level when the boundaries contain sharp corners. This is usually circumvented using many elements in the vicinity of the singular point. Therefore we modeled the stress on a plate imposing a very fine mesh at the plate tip.

An edge singularity is usually characterized by a specific exponent. Following [Pakdel and Kim, 1996], the traction in proximity to a side corner of a body can be expressed as ϵ^{α} where ϵ is the normalized distance from the border and α is an exponent between 0.5 (maximal singularity for a two-dimensional flow) and 2 (over that the drag becomes infinite). The singularity is typically calculated with the Boundary Elements Method, discretizing finer the surface close to the edge [Pozrikidis, 2002] or with a collocation-interpolation scheme [[Pakdel and Kim, 1996,].

The three plots in figure 6 show the results obtained after assuming lateral boundaries and highly resolved mesh at the edge. The von Mises stress field (second invariant of the deviatoric stress tensor) and the pressure (trace of the stress tensor) are singular at the plate extremities. The singularity quantifies the forcing of the back-flow to the migrating plate. The integration of the the singularity at the edge quantify the drag used to couple the BEM and FEM methods.

We show the comparison of the two solutions in figure 7 where we plot the evolution of the plate subjected to a body force towards the right. On the left column the BEM-FEM solution is compared with with the one obtained with a pure FEM solver (right column). The two results are in excellent agreement. Small differences are visible for the stress within the plate, due to different precision of calculating the singularity at the edge and due to the coarse resolution. The coupled solution required only 40 finite elements and 24 boundary elements while the full FEM solution needed 10000 finite elements.

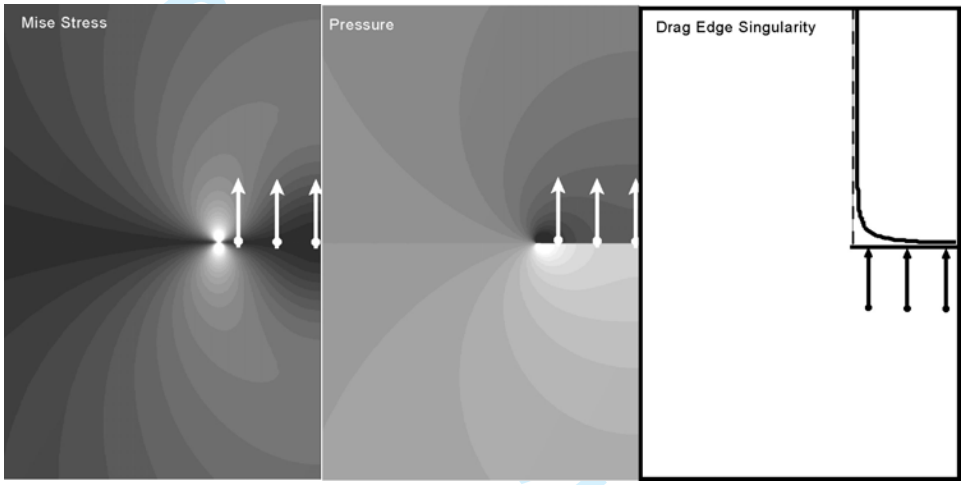

Figure 6: The three plots show the stress field induced by a plate that moves at constant velocity, far away bounded on the left side. Left panel shows the von Mises field stress (second invariant of the deviatoric part of the Cauchy stress). It tends to infinity at the edge. The panel in the center shows simply the pressure distribution, also singular at the edge: positive (black) in the front and negative (white) behind the plate. Finally the right panel plots the stress in direction of the plate motion.

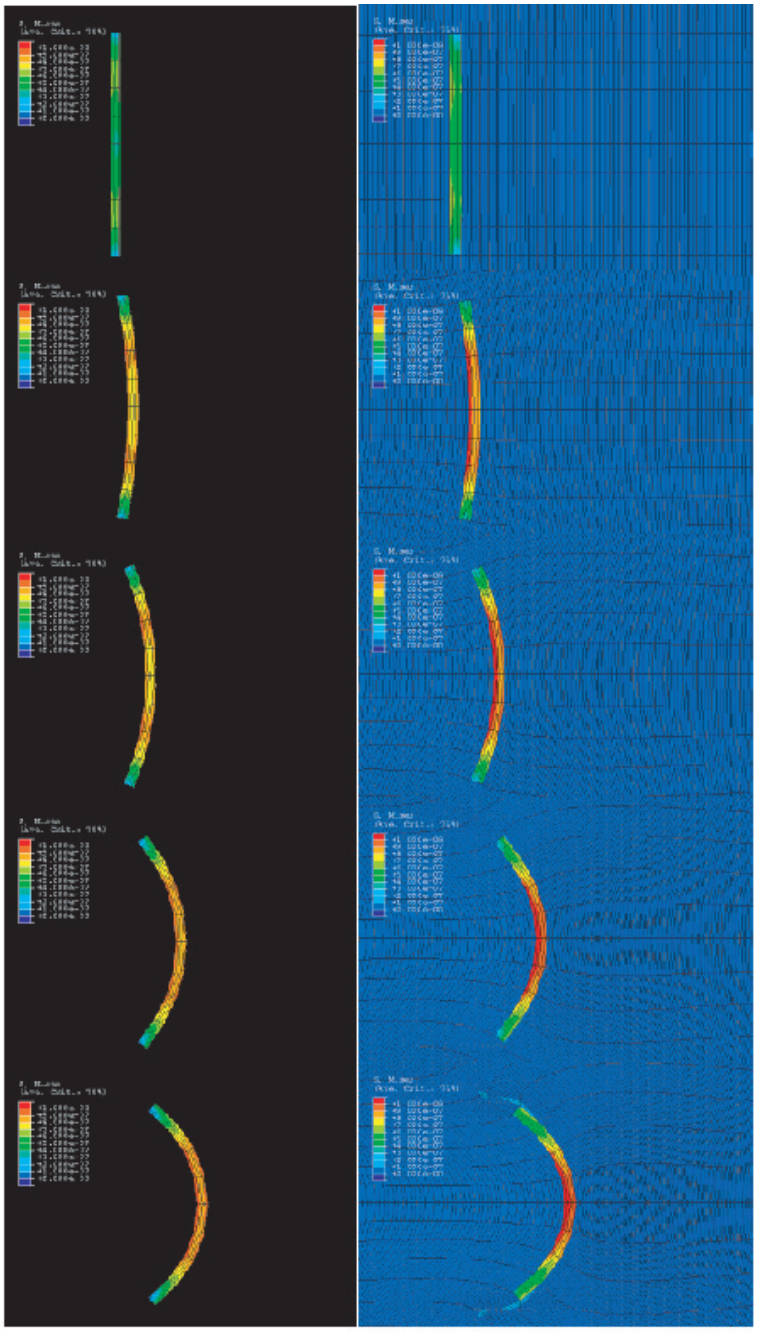

Figure 7: The evolution of a viscoelastic plate (Viscosity = 10^{23}Pas, Young Modulus = 10^{21}Pa) immersed in a viscous fluid (Viscosity = 10^{21} Pas). The sequence shown on left is obtained with the BEM-FEM simulation, while on right it is shown the benchmark calculated with the industry standard FEM code ABAQUS. Red plots 100MPa, while blue is 0MPa.

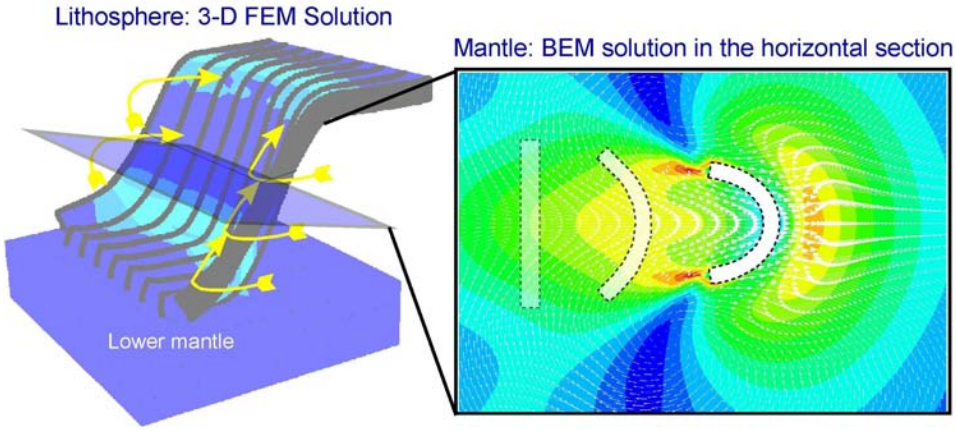

Figure 8: Subduction is modeled through the coupling of a FEM three-dimensional solver bounded at each horizontal plane by drag tensors obtained from a two-dimensional BEM solution. Left panel: colors are von Mises Stress (second invariant of the deviatoric stress) in the lithosphere. Right panel: colors are the strain in the mantle.

5 Application of BEM-FEM (2D-3D) for modeling subduction

When a plate is migrating horizontally in the mantle, the forcing exerted by the plate to the surrounding creeping flow will create a toroidal back-flow. The plate is then expected to change shape to accommodate the viscous forcing depending on the resistance to bending of the plate.

We propose here an example of how the setting proposed in the above section can be applied to estimate the deformation obtained on the migrating plate. The setup is shown in fig 8: an Implicit Finite Element (FEM) code [ABAQUS/Standard, 2000] solves for the lithosphere and an Implicit Boundary Elements (BEM) code for the mantle. We neglect the presence of the overriding plate.

We model the dynamics of subduction driven only by compositional density contrast and a gravitational body force. The initial configuration is a lithosphere where subduction is just initiated (100-150km initial depth) and then left free to sink into the surrounding mantle. A viscosity jump of 30 at 660km depth, between upper and lower mantle, is also assumed. In the above example the lithosphere rheology is viscoelastic with elasticity $E = 10^{10} Pa$ and viscosity $\eta = 10^{23} Pas$ while the mantle has a viscosity $\eta = 10^{21} Pas$.

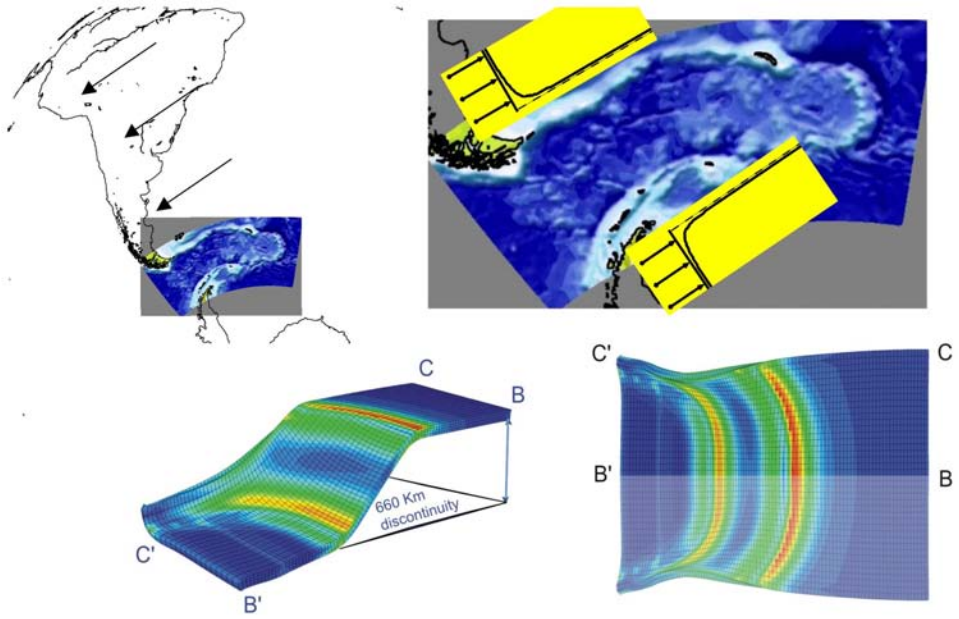

Figure 9: The southern South America displays a peculiar hook shape that could be induced by the forcing of the lateral mantle flow. The chart on the top-left shows the coast lines while arrows represent the plate motion direction. The panel on top-right displays a view of the bathymetry of the Scotia-Sandwich plates system, illustrating where the edge-forcing could play a role shaping the plate. In the bottom panel we show the lateral view and top view of the model results of a retreating plate obtained with the coupled BEM-FEM appraoch.

With this setup, models run on an Alpha architecture on a single CPU. The time required for solving the FEM mesh defined by 4x20x80 cubic elements in a pure mechanical setting (the feedback with the temperature is not considered here) is less then 1 day.

It is interesting to investigate whether our models are compatible with observation of nature. For example in figure 9 we compare our results for a subducting plate defined by viscoelastic rheology (see [Funiciello et al., 2003b] for details) and the case of southern South-America. Following the tectonic reconstruction proposed by Russo and Silver [Russo and Silver, 1994], the Eastward migration of South-American plate would displace mantle toward the sides (Caribbean at the north and Sandwich at the south). We show in figure 9 - bottom that the surface deformation calculated by our model for a generic plate is localized at the slab edge,

in agreement with the observed deformation. This hook-shaped deformation is, in its basic principles, explained by the singular stress at the slab edge (fig. 9 - top right) due to mantle back-flow. In real nature the effect is possibly amplified owing to positive feed-back of a very young subducting Sandwich subduction system producing a double hook shape.

This explanation compatible with the tectonic history of the region which suggests that the North-Scotia ridge may have been a subduction zone before becoming conservative [Thomas et al., 2003, Pelayo and Wiens, 1989]. The trench shape of such reconstruction would also match the hook shape as here proposed. Our argument is therefore that with any tectonic setting, the large amount of mantle displaced by the motion of South-American plate had to exert a forcing which generated flow and therefore a plate deformation localized at the edge of the ending plate or at the corner between the two trenches. This is confirmed by the presence of high gravity anomaly in the channel between South-America, Antarctica and Sandwich trench (see for example antwrp.gsfc.nasa.gov/apod/ap030723.html).

A quantitative comparison of the results which can be obtained with our approach was done testing a variety of slab widths and lithosphere-mantle viscosity ratios. In figure 10 we compare our results with the dataset Tovish and Schubert [Tovish and Schubert, 1978] who compiled a list of the arc curvatures (here defined as inverse of arc radius). We find that our model robustly predicts a lower bound for arc curvature. The effect of slab viscosity seems indeed to be minor whereas the mantle flow forcing is dominating. This result shows that mantle flow effects generally create a minimum curvature for arcs observed on Earth. We conclude, from this observation, that our simulation are capable to capture reasonably well the real deformation of the mantle-lithosphere feed-back but that the arc shape can be fitted only through the implementation of inhomogeneities within the lithosphere. This effect is addressed in a forthcoming paper [Morra et al., 2005].

6 Conclusions

We have shown that the BEM-FEM method has the potential for modeling the full mechanical feed-back between lithosphere and mantle. This is an ideal tool for testing conceptual models in a true geodynamics framework. This tool allows us to focus on the ”mesoscale” mechanisms that happen within the slab in a dynamical setting placed between the global mantle convection and the micro-scale mineralogical flow. The BEM-FEM approach speeds up the model for three-dimensional settings. It is possible to perform a simple three dimensional full dynamics calculation of subduction in the order of a day on a single CPU (if shell elements are employed for the lithosphere the calculation reduces to 5 hours).

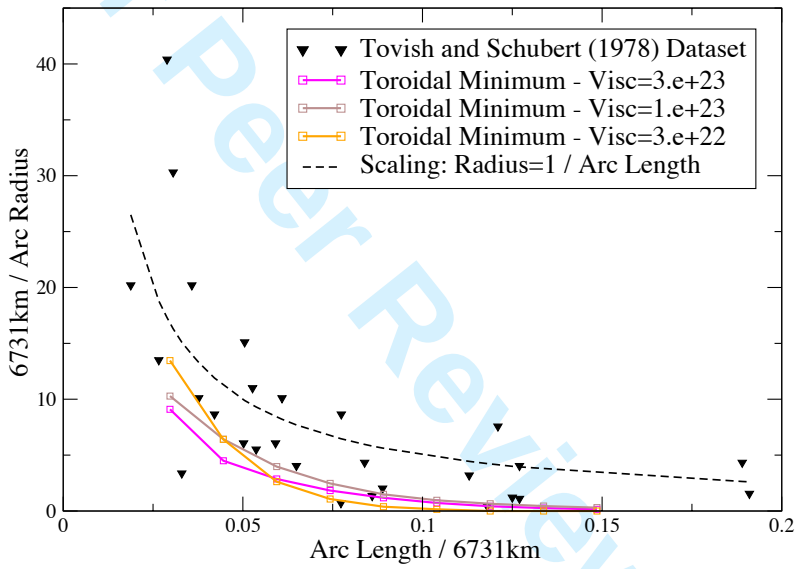

Figure 10: Plot of the normalized inverse of Arc Radius (r/AR) toward the normalized Half Arc Length (AL/r), where r=6731km. The triangles represent the 28 arcs of the dataset of Tovish and Schubert (1978). The dotted black line displays the ”mean” value for AR equal to AL. Toroidal back-flow forcing induces a curvature which fits a lower bound for observed arcs.

The method is based on an implicit coupling between BEM and FEM. The information passes between the two domains through a tensor calculated by the BEM code. This approach also overcomes a typical problem arising when coupling different codes in a staggered framework: the continuos update of the informations between the two codes requires short time increments, otherwise numerical instabilities arise [Pozrikidis, 1992]. Our BEM-FEM approach allows keeping the implicit method for both solvers, making it available for the large time step necessary for resolving the entire process of subduction.

This method is far from solving the problem of solid-fluid coupling in its most general framework. The limitations of the method mainly lie in the possibility to find a solution for the Green function of the elliptical partial differential equation solved by the Boundary Element Method. Further developments will involve the use of approximate methods as Chebychev polynomial or spectral methods for the Green functions. Furthermore improvements should involve solid-fluid boundary re-meshing.

References

[ABAQUS/Standard, 2000] ABAQUS/Standard (2000). *Theory Manual*, volume User's Manual Vol. 1, Version 6.1. Hibbit, Karlsson and Sorenson Inc.

[Bercovici, 1993] Bercovici, D. (1993). A simple model of plate generation from mantle flow. *Geophysical Journal International*, 114:635–650.

[Buiter et al., 1998] Buiter, S. J. H., Wortel, M. J. R., and Govers, R. (1998). The role of subduction in the evolution of the apennines foreland basin. *Tectonophysics*, 296(3-4):249–268. NOV 10 TECTONOPHYSICS.

[Christensen, 1996] Christensen, U. R. (1996). The influence of trench migration on slab penetration into the lower mantle. *Earth and Planetary Science Letters*, 140:27–39.

[Cizkova et al., 2002] Cizkova, H., van Hunen, J., van den Berg, A., and Vlaar, N. (2002). The influence of rheological weakening and yield stress on the interaction of slabs with the 670 km discontinuity. *EARTH AND PLANETARY SCIENCE LETTERS*, 199 (3-4):447–457.

[Davies, 1995] Davies, G. (1995). Penetration of plates and plumes through the mantle transition zone. *Earth and Planetary Science Letters*, 133:507–516.

[Faccenna et al., 1999] Faccenna, C., Giardini, D., Davy, P., and Argentieri, A. (1999). Initiation of subduction at atlantic-type margins: Insights from laboratory experiments. *Journal of Geophysical Research*, 104(B2):2749–2766.

[Funiciello et al., 2003a] Funiciello, F., Faccenna, C., Giardini, D., and Regenauer-Lieb, K. (2003a). Dynamics of retreating slabs (part 2): Insights from 3d laboratory experiments. *Journal of Geophysical Research*, 108(B4):p. art. no. 2206.

[Funiciello et al., 2003b] Funiciello, F., Morra, G., Regenauer-Lieb, K., and Giardini, D. (2003b). Dynamics of retreating slabs (part 1): Insights from 2-d numerical experiments. *Journal of Geophysical Research*, 108(B4):p. art. no. 2207.

[Gvirtzman and Nur, 1999] Gvirtzman, Z. and Nur, A. (1999). The formation of mount etna as the consequence of slab rollback. *Nature*, 401:782–785.

[Happel and Brenner, 1983] Happel, J. and Brenner, H. (1983). *Low Reynolds Number Hydrodynamics*. Martinus Nijhoff, the Hague, Netherlands.

[Hassani et al., 1997] Hassani, R., Jongmans, D., and Chery, J. (1997). Study of plate deformation and stress in subduction processes using two-dimensional numerical models. *Journal of Geophysical Research*, 102(B8):17951–17965.

[Houseman and Gubbins, 1997] Houseman, G. and Gubbins, D. (1997). Deformation of subducted oceanic lithosphere. *Geophysical Journal International*, 131:535–551.

[Jacoby, 1973] Jacoby, W. (1973). Model experiment of plate movements. *Nature-Physical Science*, 242(122):130–134.

[Kincaid and Olson, 1987] Kincaid, C. and Olson, P. (1987). An experimental study of subduction and slab migration. *Journal of Geophysical Research*, 92:13832–13840.

[Kincaid and W., 2003] Kincaid, C. and W., G. R. (2003). Laboratory models of the thrmal evolution of the mantle during rollback subduction. *Nature*, 425(6953):58–62.

[Moresi and Solomatov, 1998] Moresi, L. and Solomatov, V. (1998). Mantle convection with a brittle lithosphere: thoughts on the global tectonic styles of the earth and venus. *Geophysical Journal International*, 133(3):669–682.

[Morra et al., 2005] Morra, G., Regenauer-Lieb, K., and Giardini, D. (2005). On the curvature of oceanic arcs. *Submitted*.

[Pakdel and Kim, 1996] Pakdel, P. and Kim, S. (1996). Traction singularities on sharp corners and edges in stokes flows. *Chem. Eng. Comm.*, 148-150:257–269.

[Pelayo and Wiens, 1989] Pelayo, A. and Wiens, D. (1989). Seismotectonics and relative plate motions in the scotia sea region. *Journal of Geophysical Research - Solid Earth and Planets*, 94 (B6):7293–7320.

[Pozrikidis, 1992] Pozrikidis, C. (1992). *Boundary Integral and Singularity Methods for Linearized Viscous Flow*. Cambridge University Press.

[Pozrikidis, 2002] Pozrikidis, C. (2002). *Boundary Element Method*. Chapman and Hall/CRC.

[Regenauer-Lieb and Yuen, 2004] Regenauer-Lieb, K. and Yuen, D. (2004). Positive feedback of interacting ductile faults from coupling of equation of state, rheology and thermalmechanics. *Pysics of the Earth and Planetary Interiors*, 142(1-2):113–135.

[Russo and Silver, 1994] Russo, R. and Silver, P. G. (1994). Trench-parallel flow beneath the nazca plate from seismic anisotropy. *Science*, 263(5150):1105–1111.

[Schmeling et al., 1999] Schmeling, H., Monz, R., and Rubie, D. (1999). The influence of olivine metastability on the dynamics of subduction. *Earth and Planetary Science Letters*, 165(1):55–66.

[Shemenda, 1993] Shemenda, A. I. (1993). Subduction of the lithosphere and back arc dynamics: insights from physical modeling. *Journal of Geophysical Research*, 98(B9):16167–16185.

[Tackley, 2000a] Tackley, P. (2000a). Self-consistent generation of tectonic plates in time- dependent, three-dimensional mantle convection simulations, 1. pseudoplastic yielding. *G3*, 01(23).

[Tackley, 2000b] Tackley, P. (2000b). Self-consistent generation of tectonic plates in time- dependent, three-dimensional mantle convection simulations. 2. strain weakening and asthenosphere. *G3*, 01(25).

[Tao and O'Connell, 1993] Tao, W. and O'Connell, R. (1993). Deformation of a weak subducted slab and variation of seismicity with depth. *Nature*, 361:626–628.

[Thomas et al., 2003] Thomas, C., Livermore, R., and Pollitz, F. (2003). Motion of the scotia sea plates. *Geophysical Journal International*, 155:789–804.

[Tovish and Schubert, 1978] Tovish, A. and Schubert, G. (1978). Island arc curvature, velocity of convergence and angle of subduction. *Geophysical Research Letters*, 5(5):329–332.

[Trompert and Hansen, 1998] Trompert, R. and Hansen, U. (1998). Mantle convection simulations with rheologies that generate plate-like behaviour. *Nature*, 395:686–689.

[Yoshioka and Wortel, 1995] Yoshioka, S. and Wortel, M. J. R. (1995). 3-dimensional numerical modeling of detachment of subducted lithosphere. *Journal of Geophysical Research*, 100(B10):20223–20244.

[Zhong and Gurnis, 1995] Zhong, S. and Gurnis, M. (1995). Towards a realistic simulation of plate margins in mantle convection. *Geophysical Research Letters*, 22:981–984.